ACS Macro Letters

Letter

pubs.acs.org/macroletters

Molecular Processes Leading to Shear Banding in Well Entangled Polymeric Melts

Mouge Mohagheghi and Bamin Khomami*

Material Research and Innovation Laboratory, Department of Chemical and Bimolecular Engineering, The University of Tennessee, Knoxville, Tennessee 37996, United States

Supporting Information

ABSTRACT: We have performed hi-fidelity dissipative particle dynamics (DPD) simulations of shear flow of polymeric melts in a broad range of system sizes and two entanglement densities to determine the critical conditions for occurrence of both transient and steady shear banding. Here, we report, for the first time, simulation results that clearly demonstrate the consecutive steps leading to shear banding, that is, the stress overshoot drives locally inhomogeneous chain deformation and thus spatially inhomogeneous chain disentanglement; in turn, the localized jump in the entanglement density along the velocity gradient direction results in a considerable jump in normal stress and viscosity, which ultimately leads to shear banding. Overall, our observations are consistent with prior experimental studies, and an explanation for the stability of steady and transient shear banded flows is postulated based on the well-known interfacial stability mechanism of stratified polymeric fluids.

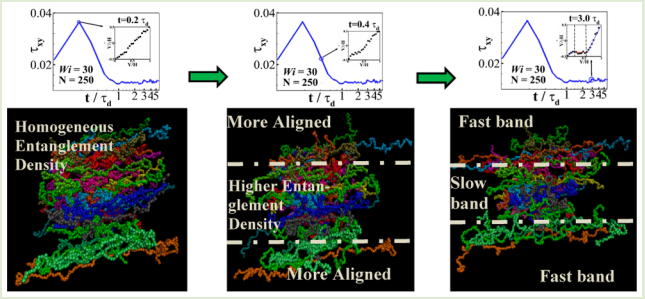

The basic foundation for modeling of entangled polymer melts has been the "Tube Theory" developed by Doi and Edwards[1] three decades ago and extensively refined since to improve its predictions of experimental measurements, that is, contour-length fluctuation and convective constraint release (CCR) were incorporated into the original "tube theory"; see refs 2 and 3, for a recent exposition of the current state of reptation theory. Despite tube theory's notable success, several key concepts including the tube field, precise definition of an entanglement and its contribution to stress remain open questions. To this end, video microscopy has been successfully employed to study the behavior and relaxation mechanism of individual chains in entangled polymeric fluids.[4,5] However, the experimental difficulties associated with tracking a sufficiently large number of single molecules in highly entangled polymeric liquids makes atomistic and mesoscopic simulations[6−9] an indispensable tool for answering the aforementioned open questions.

The original Doi−Edwards constitutive equation[1] predicts a stress maximum at the shear rate in the vicinity of the inverse of the reptation time, τ_d^{-1}. Hence, it is prone to shear banding, that is, the fluid, instead of flowing with a uniform velocity in a unidirectional shear flow, separates into distinct fast and slow flowing regimes. Incorporation of CCR broadens the relaxation spectrum, thereby reducing the possibility of shear banding. However, ample experimental observations via particle tracking velocimetry, most notably from Wang's group,[10−12] have documented the existence of steady and transient shear banding in unidirectional shear flow of entangled polymeric fluids (1 to 2 × 10^6 g/mol polybutadiene solutions).

Continuum level linear stability analyses with the most advanced tube-based models, such as the Rolie−Poly model,[13] have also demonstrated the existence of transient shear banding for both monotonic and nonmonotonic shear stress−shear rate flow curves.[14−16] However, the linear stability predictions are not conclusive since they are very sensitive to the assumed rate of CCR. Thus, even the most advanced reptation based constitutive equations require additional molecular level information before conclusively addressing flow instability and shear banding in this class of flows. To this end, development of atomistic or coarse-grained simulation techniques could play a central role in determination of the critical condition for onset of shear banding as well as its mechanism. In fact, a recent study has demonstrated the utility of Non-Equilibrium Molecular Dynamics (NEMD) simulations in predicting shear banding in planar Couette flow of entangled polymeric melts, modeled as bead−spring chains.[17] Both transient and steady shear banding for nonmonotonic shear stress−shear rate flow curve were observed in a start-up flow of polymeric fluids with equilibrium entanglement density of 10.

Although to date the existence of shear banding in entangled polymeric melts has been documented in one molecular simulation and in many experiments, the molecular mechanism for this intriguing phenomenon is not known. In fact, today the origin of shear banding is one of the most highly debated topics in the rheology community. To this end, we have performed hi-

Received: April 9, 2015
Accepted: June 12, 2015
Published: June 15, 2015

DOI: 10.1021/acsmacrolett.5b00238
ACS Macro Lett. 2015, 4, 684−688

fidelity coarse-grained dissipative particle dynamics (DPD) simulations in a broad range of system sizes (various box sizes) and two entanglement densities to determine the critical conditions for occurrence of both transient and steady shear banding. Overall, our aim is to pave the way for a mechanistic understanding of shear banding in entangled polymeric fluids via detailed analysis of flow-microstructure coupling. In this communication we report, for the first time, simulation results that describe the progression to macroscopic shear banding in well entangled polymer melts. Specifically, during stress relaxation in a typical start-up setting, spatially inhomogeneous chain disentanglement in the velocity gradient direction acts as an intermediate step between a stress overshoot and the development of a banded velocity profile.

Motivated by a well-established prior study,[18] we have developed and benchmarked a highly efficient massively parallel DPD code for entangled polymeric liquids. In these simulations, the topological constraints created by surrounding chains are satisfied by choosing an appropriate conservative force amplitude complemented by a reasonable description of bond stretching (for more information, see ref 18). Mass m, length r_c, and energy k_BT are the base units; thus, the DPD time scale is given by $\tau = (mr_c^2/k_BT)^{1/2}$. The DPD formulation[19,20] consists of pairwise conservative (F^C), dissipative (F^D), and random (F^R) forces applied between all the beads within a certain cut-off distance r_c. These forces are given by

$$\begin{cases} F_{ij}^{C} = a_{ij}\left(1 - \dfrac{r_{ij}}{r_c}\right)\vec{e}_{ij}, & r_{ij} \le r_c \\ 0, & r_{ij} > r_c \end{cases}$$

$$F_{ij}^{D} = -\gamma\omega^{D}(r_{ij})(\vec{v}_{ij}\cdot\vec{e}_{ij})\vec{e}_{ij}, \quad F_{ij}^{R} = \sigma\zeta_{ij}\omega^{R}(r_{ij})\vec{e}_{ij}$$

where

$$\vec{r}_{ij} = \vec{r}_i - \vec{r}_j, \quad |\vec{r}_{ij}| = r_{ij}, \quad \vec{e}_{ij} = \vec{r}_{ij}/r_{ij}, \quad \vec{V}_{ij} = \vec{V}_i - \vec{V}_j$$

a_{ij} is the maximum repulsion between particles i and j. The weighting functions, ω^D and ω^R, as well as γ and σ, are related through the fluctuation−dissipation theorem. ζ_{ij} is a randomly fluctuating variable with Gaussian statistics. The beads are connected using harmonic springs,[18] and a small bending potential[21] is effective between three consecutive beads.

We chose the following: $a = 200$, k (spring constant) = 400, k_b (bending stiffness) = 2.0, $r_{eq} = 0.95$, $\gamma = 4.5$, $\rho = 1.0$, and $\delta t = 0.012$ in the DPD units. The correct scaling of radius of gyration and longest relaxation time with molecular weight confirms accurate inclusion of excluded volume and hydrodynamic correlations in the simulations, thus, proves the fidelity of our DPD model. The aforementioned DPD simulator, in conjunction with Lees-Edwards boundary condition,[22] has been used to study shear banding in the planar Couette flow of entangled polymeric systems of $N = 200$ ($\langle Z\rangle = 13$ entanglements per chain at equilibrium) and $N = 250$ ($\langle Z\rangle = 17$ entanglements per chain at equilibrium) with 1250 and 705 chains, respectively, in a canonical (NVT) ensemble. The number of entanglements in the aforementioned systems is close to the lower range of experimental entanglement densities where shear banding has been observed. The equations of motion were integrated by the velocity-Verlet algorithm. The results reported are from a simulation box with an aspect ratio of 2.5:1:1 with a larger dimension in the flow direction, x. Normal dimensions to the flow direction are at least twice the average equilibrium chain end-to-end distance. To achieve steady state velocities, shear and first normal stresses, simulations up to 6× the longest relaxation time of the system have been performed. Considering the large size of the simulation box, accurate temporal ensemble averages were obtained over 0.1 τ_d. The accuracy of the results was further verified by performing simulations with different initial conditions and box sizes. The reported results are free of any artifacts associated with the box size. Please refer to the SI for a complete discussion of the influence of box size on the observed shear banded structures. Moreover, our simple shear simulation results are fully consistent with NEMD computations of Nafar et al.[23] It should also be noted that the entanglement densities reported herein were determined by using the Z1 code developed by Kröger et al.[24,25]

The steady shear stress as a function of shear rate for chains with 200 and 250 beads is depicted in Figure 1. In this figure

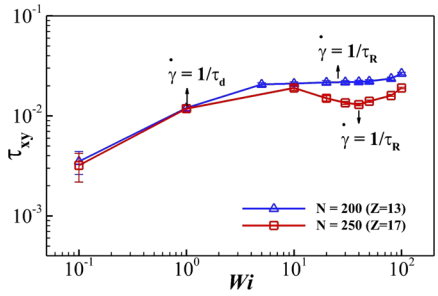

Figure 1. Steady shear stress as a function of Weissenburg number. Rouse time, τ_R is estimated via $(\tau_d/\tau_R) = 3Z$.

the shear rate is nondimensionalized by the equilibrium longest relaxation time of each system, that is, τ_{d0} ($Wi = \dot{\gamma}\tau_{d0}$) and shear stress value is reported in DPD unit. In what follows, the longest relaxation time of the system or the disengagement time under flow at a given shear rate is labeled as τ_d. In general, the disengagement time is calculated by fitting the autocorrelation function of unit end-to-end vector with an exponential function.

We have observed steady shear banding in the most entangled system, $N = 250$ at $Wi = 30$ and 40, that is, shear rate regime of, $\tau_d^{-1} < \dot{\gamma} < \tau_R^{-1}$. Henceforth, the flow dynamics in the most entangled system has been scrutinized via detailed examination of the temporal evolution of velocity profile and shear stress. As depicted in the inset of Figure 2a, a linear velocity profile is observed at the stress overshoot ($t = 0.2\tau_d$), however, and at $t = 0.4\tau_d$, localized perturbations in the velocity profile are observed. These perturbations grow and lead to the incipient stratified flow/shear banded structures at $t = 0.6\tau_d$. In turn, the slow (low shear rate) and fast (high shear rate) bands continue to develop ($2\tau_d < t < 6\tau_d$); specifically, the thickness of the slow band gradually increases until it occupies nearly half of the box. At this point, the steady shear banded structure is realized.

As the existence of steady shear banding has been clearly demonstrated for the most entangled system studied, our primary goal hereafter is to gain insight into the molecular mechanism of shear banding. To this end, first topological measures of the entanglement network as a function of flow strength have been investigated. In general, the probability distribution function of the entanglement density $P(Z)$, follows a Poisson distribution at equilibrium[6] as well as under flow

DOI: 10.1021/acsmacrolett.5b00238
ACS Macro Lett. 2015, 4, 684−688

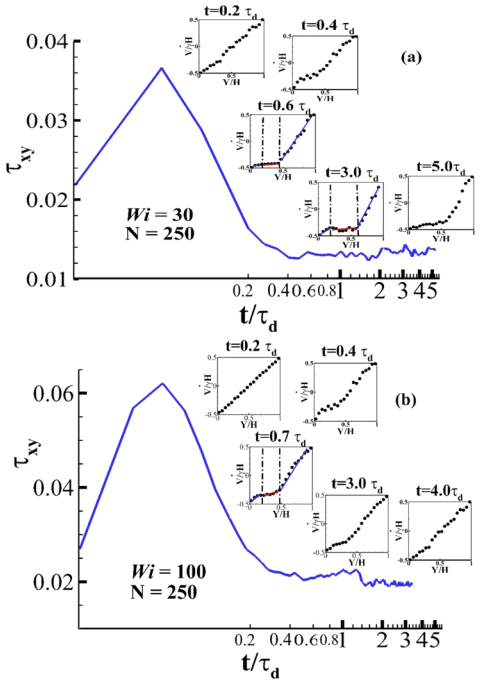

Figure 2. (a, b) Temporal evolution of shear stresses and velocity profiles: (a) steady shear banding; (b) transient shear banding. Velocity profiles are shown in the inset with their time labels. The time, t, the horizontal axis in the figure subsets (a) and (b) is scaled with the disengagement time at the applied shear rate. The minor ticks in the figure represent $0.2\tau_d$.

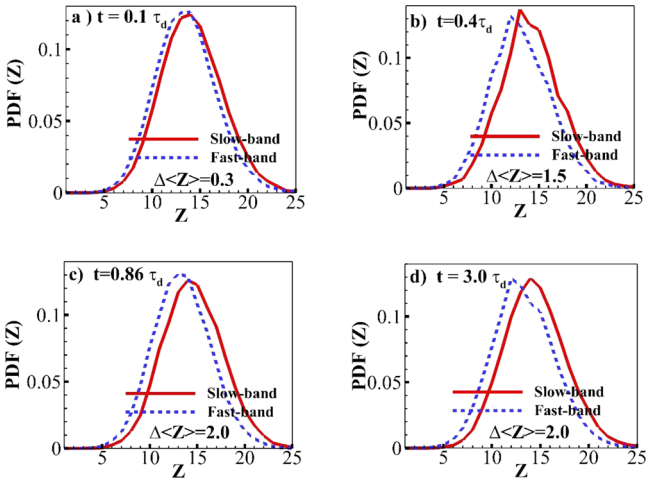

Figure 3. (a–d) Entanglement probability distribution function at different times for Wi = 30. The red and dashed blue lines, respectively, show the regions of the flow that are eventually occupied by the slow and fast bands after $0.6\tau_d$; $\Delta Z = \langle Z\rangle$slow band $- \langle Z\rangle$fast band.

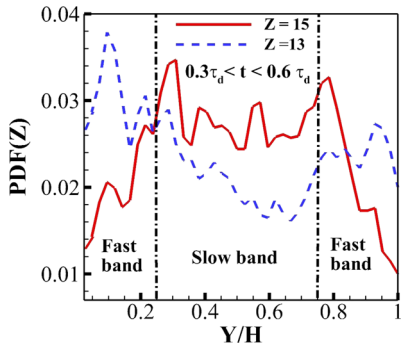

Figure 4. Spatial probability distribution function of two specific entanglement points, 13 and 15, along the velocity gradient direction Y, during transient time (time average between 0.3 and 0.6τd). The vertical dashed lines show the interface between the slow and fast bands. Note this spatial pdf belongs to the steady shear banding case, N = 250 and Wi = 30.

conditions, as shown by ref 6. A detailed examination of the number of entanglements, and the entanglement distribution reveals significantly different results in the regions that are eventually occupied by the slow and fast bands at steady state. Specifically, after the stress overshoot ($t > 0.2\tau_d$), but long before the incipient stratified flow/shear banded structure is observed ($t < 0.6\tau_d$), the entanglement distribution function as well as the average entanglement density ($\langle Z\rangle$) become different in the aforementioned regions. This topological feature continues as long as shear banding exists (see Figure 3). This finding underscores the fact that inhomogeneous flow-induced disentanglement in the velocity gradient direction occurs (see Figure 4) before the shear banded structure is observed. Specifically, the less entangled chains populate the faster velocity band, and the more entangled chains are within the slower band.

We hypothesize that the origin of inhomogeneous chain disentanglement in the velocity gradient direction is a consequence of stress overshoot and subsequent stress relaxation caused by rapid and continuous changes in molecular configuration including chains orientation and stretch. During stress relaxation, chain orientation is not a dominant relaxation mechanism; hence, spatially inhomogeneous deformation of the chains occurs between $t \geq 0.2\tau_d$ and $t \leq 0.4\tau_d$ after the stress maximum (see Figure 5a,b), leading to distinct chain topologies and commensurate inhomogeneous chain entanglement densities. This hypothesis is consistent with the free energy calculation of Marrucci and Grizzuti[26] for the Doi–Edwards model. Specifically, they have shown that for shear strain $\gamma > 2$ curvature of the free energy is negative. This condition in turn leads to "inhomogeneous deformation" unless relaxation mechanisms, including orientation, occur to such an extent as to significantly reduce the free energy. However, the latter can only occur at very large values of shear rates. Our simulations are also in agreement with the aforementioned postulate that is in the presence of considerable stress overshoot (as evidenced in Figure 2 for $Wi \geq 30$) inhomogeneous chain disentanglement in the velocity gradient direction is created; moreover, for very large shear rates, that is, $Wi \geq 200$, chain orientation and the associated relaxation mechanism occur so rapidly that the formation of inhomogeneous chain entanglement densities is essentially prevented (see Figures S2 and S3 in the SI).

It is a well-known fact in theories of flowing polymeric melts that entanglement density determines the elastic and viscous behavior of the fluid. To this end, the observed localized jump in entanglement density results in a pronounced jump in the first normal stress N1 and localized differences in viscosity along the velocity gradient direction. A prototypical temporal evolution of first normal stress in the aforementioned region and its difference between the less elastic (slow band) and more elastic (fast band) bands for a steady shear banded flow is shown in Figure 6. In general, due to the increased alignment of the chains in the flow direction during start-up, first normal

DOI: 10.1021/acsmacrolett.5b00238
ACS Macro Lett. 2015, 4, 684–688

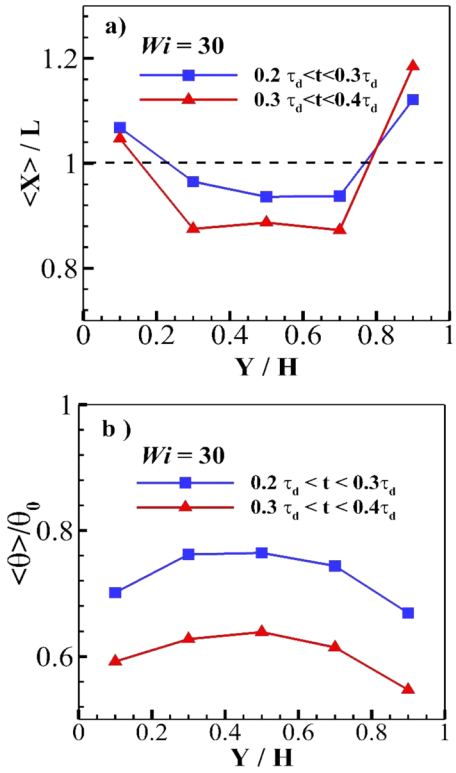

Figure 5. (a) Average chain extension in the flow direction scaled by L along the velocity gradient direction, L is the magnitude of chain end-to-end distance projection in the x direction at equilibrium. (b) Mean chain angle calculated with respect to the flow direction along the velocity gradient direction normalized by the θ_0, θ_0 is the average chain angle with respect to the x direction at equilibrium. Y is scaled by the box size, H.

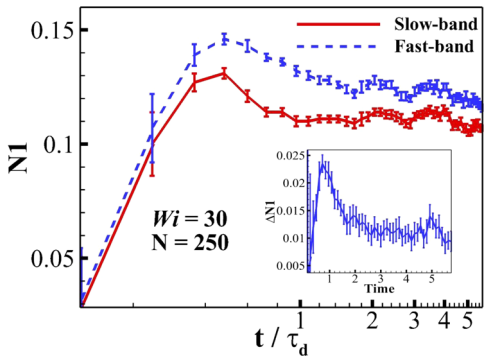

Figure 6. Temporal evolution of first normal stress of steady shear banded structures. The difference of N1 between the two bands (ΔN1) is shown in the inset. During stress relaxation when chain disentanglement occurs ($t \leq 1\tau_d$), ΔN1 reaches its utmost value, 23% of the average N1 of the system, and then decreases to 14% of the average N1 at the steady state. The time, t, the horizontal axis, is scaled with the disengagement time at the applied shear rate.

stress rises in both regions. Moreover, based on a polymer chain configurational analysis, the chains with less entanglement are more aligned in the flow direction as compared to more entangled chains. Hence, the jump across the interface, that is, ΔN1, and the associated viscosity difference grows as a function of time until it reaches its steady value. Specifically, after the stress overshoot, at $t = 0.4\tau_d$, the localized jump in the entanglement density gives rise to a significant ΔN1, that is, 13% of the average first normal stress and commensurate perturbations in the velocity profile in Figure 2a. The aforementioned localized nonuniform viscosity and elasticity difference give rise to a stratified shear flow. We hypothesize that if this stratified flow is stable to the interfacial disturbances, it evolves over time until a steady shear banded profile is realized. This sequence of events is clearly depicted in the insets of Figure 2a starting at $t = 0.6\tau_d$ and culminating at $t = 5\tau_d$. On the other hand, if the stratified flow is unstable to interfacial disturbances, interfacial perturbations develop and grow in time, leading to interfacial mixing and destruction of a highly localized jump in entanglement density in the velocity gradient direction. Hence, the stratified flow will return back to a uniform shear flow, as depicted in the insets of Figure 2b.

The rational suggested above clearly assumes that hydrodynamic modes are supported in the simulation box. However, it should be noted that this is only a postulate and detailed examinations are required based on extensive continuum level analyses which is beyond the scope of this paper. Henceforth, the interfacial stability of the sequence of stratified flows leading either to a steady banded structure or homogeneous shear flow will be scrutinized. In the limit of vanishing Reynolds number (Re) and negligible interfacial tension, the parameter space that determines the interfacial stability of stratified flows consists of viscosity, elasticity and depth ratio. Specifically, in this class of flows two general roles exists:[27−30] (1) when the less viscous fluid is thin compared to the more viscous fluid, the interface is stable, the so-called "thin layer effect",[27] and (2) when the more elastic layer is the majority component, elasticity stratification is stabilizing.[28] As shown in the inset of Figure 2a, where a steady shear banded structure is observed, the slow band is the more viscous and less elastic layer and occupies less than half of the box volume in the incipient stratified flow. Hence, one has to determine the relative importance of viscosity and elasticity stratification on the overall stability of the interface. Fortunately, Su and Khomami[29] have already performed a comprehensive study of the interfacial instability of stratified polymeric flows. Specifically, they have demonstrated that for depth ratios ($\varepsilon = d_{\text{more viscous}}/d_{\text{less viscous}}$) larger than 0.5 and elasticity ratios ($\text{EL} = \text{N1}_{\text{more elastic}}/\text{N1}_{\text{less elastic}}$) of order one, the viscosity ratio ($R = \eta_{\text{more viscous}}/\eta_{\text{less viscous}}$) should be larger than ∼6 for the interface to be stable (for more information, please check Figure 2b in ref 30). Using the analogy explained in the steady shear banding case, our incipient stratified flow and its subsequent evolution to the final steady shear banded flow is stable since $1.17 < \text{EL} < 1.3$, $0.8 < \varepsilon < 1$, and $9.5 < R < 13$, that is, under these conditions interfacial modes are suppressed in the incipient banded structure and its subsequent flow configurations. Hence, the observation of a steady shear banding evolution is fully consistent with the interfacial stability analysis of stratified viscoelastic polymeric flows.

Transient shear banding has also been observed in both systems ($N = 200$ and 250) considered, but only at shear rates larger than the inverse of rouse time of each system (see Figure 2b for a representative case). Although the progression to banding, namely, observation of inhomogeneous entanglement density in the velocity gradient direction, jump in the first normal stress and the commensurate viscosity difference is identical to the case where steady shear banding has been observed, the incipient stratified flow is short-lived and it returns to a homogeneous shear flow at $\sim 4\tau_d$. This short lifetime of the banded structures is due to the fact that the stratified flow is interfacially unstable. Specifically, the incipient

DOI: 10.1021/acsmacrolett.5b00238
ACS Macro Lett. 2015, 4, 684−688

stratified flow and all observed short-lived banded structures are unstable to interfacial modes as $1.05 < EL < 1.08$, $4 < R < 5$, and $0.53 < \varepsilon < 0.66$; hence, interfacial disturbances amplify and lead to interfacial mixing that, in turn, reduces the jump in N1 and difference in viscosity until the first normal stress and viscosity difference vanishes and flow returns to its homogeneous linear state (for more details on transient shear banding, please refer to the Supporting Information). Overall, our observation of transient shear banding is not only consistent with earlier experimental findings, but also clearly depicts that transient shear banding can occur for both monotonic and nonmonotonic flow curves in the region where shear stress is an increasing function of shear rate.

In conclusion, we have found the progression to shear banding in highly entangled polymeric fluids based on the one to one correspondence between flow-induced microstructural evolution and fluid rheological properties. Specifically, in the regime near or after the stress over shoot inhomogeneous flow-induced entanglement densities in the velocity gradient direction is observed giving rise to a discernible localized jump in the first normal stress and a commensurate difference in viscosity which leads to formation of a stratified shear flow. In other words, the transition from a homogeneous flow to macroscopic banding evolves through the spatially inhomogeneous entanglement density as it enhances the viscoelastic stratification of the flow in the well entangled polymeric melts. Moreover, the stability of steady and transient shear banded structures has been rationalized based on the interfacial stability of the stratified flow. Overall, this study has paved the way for mechanistic understanding of occurrence of shear-banded structures in entangled polymeric fluids.

■ ASSOCIATED CONTENT

Supporting Information

Details of transient shear banding and clear box size effects are discussed. The Supporting Information is available free of charge on the ACS Publications website at DOI: 10.1021/acsmacrolett.5b00238.

■ AUTHOR INFORMATION

Corresponding Author

*E-mail: bkhomami@utk.edu.

Notes

The authors declare no competing financial interest.

■ ACKNOWLEDGMENTS

The authors would like to acknowledge the National Science Foundation (EPS-1004083) as well as the University of Tennessee and Oak Ridge National Laboratory Joint Institute for Computational Sciences for the support of this work.

■ REFERENCES

(1) Doi, M.; Edwards, S. F. *The Theory of Polymer Dynamics*; Clarendon Press: U.K., 1988.
(2) McLeish, T. C. B. *Adv. Phys.* **2002**, *51*, 1379−1527.
(3) Larson, R. G.; Sridhar, T.; Leal, L. G.; McKinley, G. H.; Likhtman, A. E.; McLeish, T. C. B. *J. Rheol.* **2003**, *47* (3), 809−818.
(4) Teixeira, R. E.; Dambal, A. K.; Richter, D. H.; Shaqfeh, E. S. G.; Chu, S. *Macromolecules* **2007**, *40* (7), 2461−2476.
(5) Robertson, R. M.; Smith, D. E. *Phys. Rev. Lett.* **2007**, *99* (12), 126001.
(6) Baig, C.; Mavrantzas, V. G.; Kröger, M. *Macromolecules* **2010**, *43* (16), 6886−6902.
(7) Dambal, A.; Kushwaha, A.; Shaqfeh, E. S. G. *Macromolecules* **2009**, *42* (18), 7168−7183.
(8) Kim, J. M.; Edwards, B. J.; Keffer, D. J.; Khomami, B. *J. Rheol.* **2010**, *54* (2), 283−310.
(9) Kushwaha, A.; Shaqfeh, E. S. G. *J. Rheol.* **2011**, *55* (3), 463−483.
(10) Tapadia, P.; Ravindranath, S.; Wang, S.-Q. *Phys. Rev. Lett.* **2006**, *96* (19), 196001.
(11) Ravindranath, S.; Wang, S.-Q.; Olechnowicz, M.; Quirk, R. P. *Macromolecules* **2008**, *41* (7), 2663−2670.
(12) Wang, S.-Q.; Ravindranath, S.; Boukany, P.; Olechnowicz, M.; Quirk, R. P.; Halasa, A.; Mays, J. *Phys. Rev. Lett.* **2006**, *97* (18), 187801.
(13) Likhtman, A. E.; Graham, R. S. *J. Non-Newtonian Fluid Mech.* **2003**, *114* (1), 1−12.
(14) Adams, J. M.; Fielding, S. M.; Olmsted, P. D. *J. Rheol.* **2011**, *55* (5), 1007−1032.
(15) Adams, J. M.; Olmsted, P. D. *Phys. Rev. Lett.* **2009**, *102* (6), 067801.
(16) Olmsted, P. *Rheol. Acta* **2008**, *47* (3), 283−300.
(17) Cao, J.; Likhtman, A. E. *Phys. Rev. Lett.* **2012**, *108* (2), 028302.
(18) Nikunen, P.; Vattulainen, I.; Karttunen, M. *Phys. Rev. E* **2007**, *75* (3), 036713.
(19) Hoogerbrugge, P. J.; Koelman, J. M. V. A. *Europhys. Lett.* **1992**, *19* (3), 155.
(20) Español, P.; Warren, P. *Europhys. Lett.* **1995**, *30* (4), 191.
(21) Sirk, T. W.; Slizoberg, Y. R.; Brennan, J. K.; Lisal, M.; Andzelm, J. W. *J. Chem. Phys.* **2012**, *136* (13), 134903.
(22) Lees, A. W.; Edwards, S. F. *J. Phys. C* **1972**, *5* (15), 1921.
(23) Nafar Sefiddashti, M. H.; Edwards, B. J.; Khomami, B. *J. Rheol.* **2015**, *59* (1), 119−153.
(24) Karayiannis, N. C.; Kröger, M. *Intl. J. Mol. Sci.* **2009**, *10* (11), 5054−5089.
(25) Shanbhag, S.; Kröger, M. *Macromolecules* **2007**, *40* (8), 2897−2903.
(26) Marrucci, G.; Grizzuti, N. *J. Rheol.* **1983**, *27* (5), 433−450.
(27) Ganpule, H. K.; Khomami, B. *J. Non-Newtonian Fluid Mech.* **1999**, *81* (1−2), 27−69.
(28) Su, Y. Y.; Khomami, B. *Rheol. Acta* **1992**, *31* (5), 413−420.
(29) Su, Y. Y.; Khomami, B. *J. Rheol.* **1992**, *36* (2), 357−387.
(30) Renardy, Y. *J. Non-Newtonian Fluid Mech.* **1988**, *28* (1), 99−115.

DOI: 10.1021/acsmacrolett.5b00238
ACS Macro Lett. 2015, 4, 684−688